Prediction of Wind Speed, Direction and Diffusivity under Neutral Conditions for Tall Stacks

NIRUPAMA RAGHAVAN AND SWATI BASU

Centre for Atmospheric Sciences, Indian Institute of Technology, India

(Manuscript received 28 February 1987, in final form 22 August 1987)

ABSTRACT

A one dimensional model of the neutral planetary boundary layer is used to predict the wind velocity and coefficient of eddy diffusivity throughout the 2-km planetary boundary layer. Comparison with routine radiosonde observations show that at 500 m, the model predictions of wind speed are within 1.2σ of the observed values where σ is the probable error of the observed values. An interesting correlation between the height of maximum diffusion and length scale (u_*/f) of the neutral boundary layer has emerged out of this study.

The velocity and diffusivity profiles from the PBL model are then used in the solution of a three-dimensional advection diffusion equation for the dispersal of nonreactive pollutants in the atmosphere. The results indicate that it is possible to select stack heights to ensure maximum dilution of a pollutant immediately on release and thereby minimize its long-range transport.

1. Introduction

In impact analysis studies associated with the siting of major industrial plants, the two most important parameters required are the wind velocity at stack height and the coefficient of eddy diffusivity. These are seldom available at the height of interest. Thus, most impact analyses use 10-m wind roses and Pasquill's dispersion parameters, which are combined with a power law profile to give the input parameters. This approach is limited in its applicability on two accounts:

(i) The power law does not give the changing direction of wind with height. Predicted concentration patterns for distances longer than 10 km, therefore, can be widely in error.

(ii) Ten m windrose and Pasquill stability parameters are time-averaged quantities. While these may yield reasonable estimates of annual mean concentrations, they would yield short term concentrations that would be grossly in error (Draxler, 1979).

This study uses a more realistic formulation to obtain the wind velocity and the coefficient of eddy diffusivity at stack height, under neutral conditions. This case is especially important for the transport of emissions from large power plants near cities, over which the atmosphere is neutral for a large fraction of the day as compared to its rural counterpart (Padmanabhamurty and Gupta, 1978). Long range transport of pollutants has gained importance in view of the precipitation of acidic rain in locations far from regions of high SO_2 release.

2. Model formulation

The neutral boundary layer which is characterized by horizontal homogeneity in wind and temperature is the simplest configuration that can be assumed for the PBL. This configuration is valid over terrain that is horizontally homogeneous with respect to its surface roughness and temperature. The momentum equations for mean quantities for such a planetary boundary layer are

$$\frac{\partial u}{\partial t} = f(v - v_g) + \frac{\partial}{\partial z}\left(K_m \frac{\partial u}{\partial z}\right), \tag{1}$$

$$\frac{\partial v}{\partial t} = -f(u - u_g) + \frac{\partial}{\partial z}\left(K_m \frac{\partial v}{\partial z}\right), \tag{2}$$

with the usual notation.

The structure of the neutral boundary layer has been determined by using a variety of forms for the K-profile and solving for Eqs. (1) and (2) (Estoque, 1974).

A simplified closure scheme using the turbulent kinetic energy equation (TKE) is capable of simulating most of the properties of the PBL with an accuracy comparable to the higher order closure (Rao and Snodgrass, 1981). This involves the solving of one additional time dependent equation,

$$\frac{\partial e}{\partial t} = K_m\left\{\left(\frac{\partial u}{\partial z}\right)^2 + \left(\frac{\partial v}{\partial z}\right)^2\right\} + \frac{\partial}{\partial z}\left(K_m \frac{\partial e}{\partial z}\right) - \frac{(be)^{3/2}}{l_\epsilon}, \tag{3}$$

where e is the turbulent kinetic energy. The last term in the TKE equation denotes the viscous dissipation

Corresponding author address: Dr. Nirupama Raghaven, Nehru Planetarium, Jawaharlal Nehru Memorial Fund, Teen Murti House, New Delhi—110011, India.

of the turbulent kinetic energy, l_ϵ is the length scale associated with dissipation, and b (=0.2) is a constant.

The above set of equations is closed with

$$K_m = l_m(be)^{1/2}, \tag{4}$$

where l_m is the mixing length for eddy diffusion of momentum. In the present work, the mixing length is assumed to consist of two parts: (i) a length characteristic of the size of eddies in the surface layer; and (ii) a limiting mixing length λ in the Ekman layer. In the surface layer which extends to a height of a few tens of meters from the ground, the mixing length is proportional to the height z. In the Ekman layer, the mixing length cannot grow indefinitely with increasing height and hence it is to be limited by the limiting value $\lambda = 0.0004G/f$ where $G = (u_g^2 + v_g^2)^{1/2}$ is the geostrophic wind, and f is the Coriolis parameter (Blackadar, 1962).

Thus the mixing length l_m is given by

$$\frac{1}{l_m} = \frac{1}{\lambda} + \frac{1}{k(z + z_0)}, \tag{5}$$

where $k = 0.40$ is the Von Karman constant and z_0 is the surface roughness. This TKE closure is similar to that used by Delage (1974), Nieuwstadt and Driedonks (1979), and Rao and Snodgrass (1981). The boundary conditions are

$$u = 0, \quad v = 0, \quad \frac{\partial e}{\partial z} = 0 \quad \text{at} \quad z = 0,$$

$$u = G, \quad v = 0, \quad \frac{\partial e}{\partial z} = 0 \quad \text{at} \quad z = \delta \text{ (PBL height)}.$$

Here, δ is the PBL height (=2 km) where generally the commencement of geostrophic balance takes place.

3. Comparison with observations

It is important to test how the model predictions of wind speed and direction compare with observations. The TKE closure model has been used to predict the 10- and 500-m wind speeds and directions and is compared with observations obtained from routine radiosonde observations at 1200 UTC for Delhi. The criteria used for selecting observations for comparison are

(i) The observed lapse rate is approximately adiabatic.

(ii) Wind speed and direction observations are available at the two heights, viz., 10 and 500 m.

(iii) No synoptic scale disturbances are present.

Thus, the most suitable periods for comparison are postmonsoon and winter months.

The observed wind speed and direction at 800 mb level was used as the geostrophic wind G for model calculations. Figures 1a and b are scatter plots of the observed and predicted 10 m wind speed and the cross-isobar angle α at the same height. For the range of geostrophic winds observed, the model predictions are

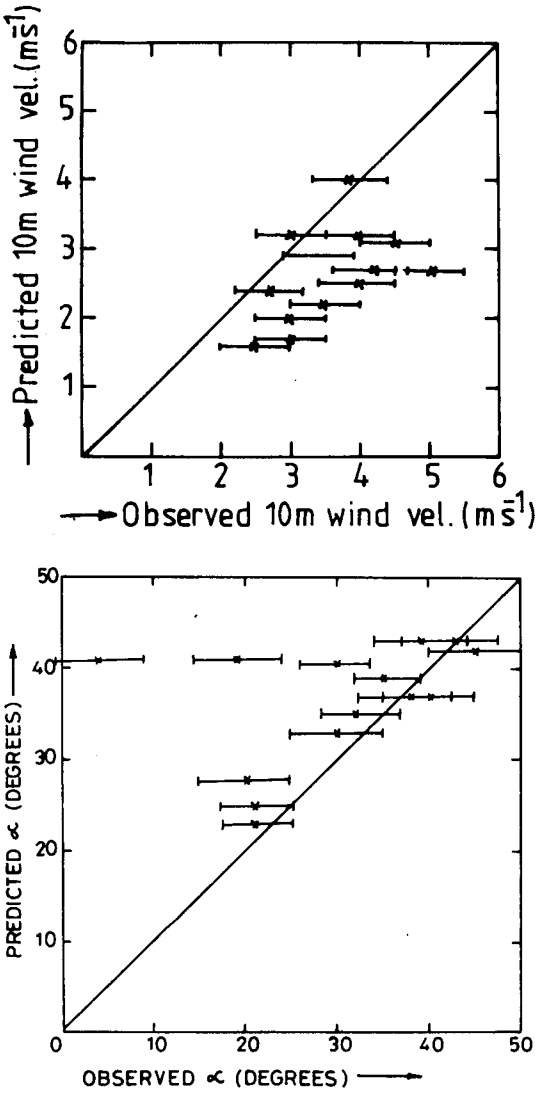

FIG. 1. Comparison of observed and predicted (a) wind speeds at 10 m height, and (b) cross-isobar angles at 10 m height.

fair. Predictions of both wind speed and α fall within the limits of observational error indicated by the error bar. Figures 2a and b compare the same parameters at 500 m. Here, speeds predicted by the model are systematically higher but within 20% of the observed values. The cross-isobar angle predictions are less satisfactory, within 2σ of the observed values. Here σ is the probable error of the observed values. In any event this is a considerable improvement over using 10-m wind directions which may differ from the 500-m directions by as much as 45°.

A further check on the model was made by calculating the drag coefficient for the experimental observations analyzed by Csanady (1967). The roughness length, geostrophic wind and the Coriolis parameter corresponding to each experiment were used as input

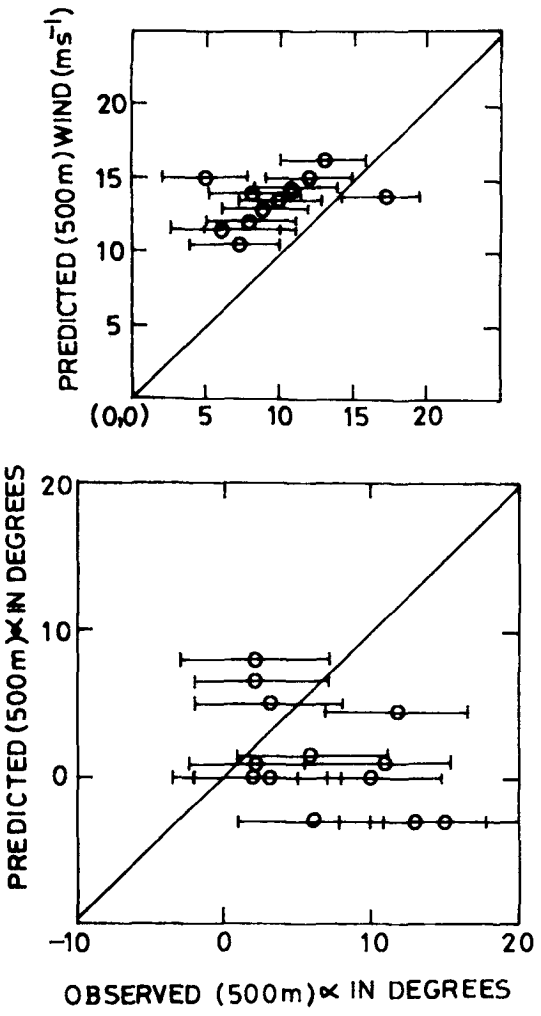

FIG. 2. (a) As in Fig. 1(a) but at 500 m height. (b) As in Fig. 1(b) but at 500 m height.

parameters. From the steady state velocity profile given by the model, the ratio of the frictional velocity to the geostrophic wind G was calculated as a function of logRo, where $\mathrm{Ro} = G/fz_0$ is the surface Rossby number. Figure 3 shows the model generated relation between logRo and u_*/G. Also plotted are the experimental values listed by Csanady (1967). Over the entire range of Ro, the curve calculated by the present model closely follows the experimental values. Shown for comparison is the model calculation of Estoque (1974). The latter model is similar to the present one except that instead of the TKE closure, the system of equations are closed with

$$K_m = l^2\left[\left(\frac{\partial u}{\partial z}\right)^2 + \left(\frac{\partial v}{\partial z}\right)^2\right]^{1/2}.$$

It is clear from Fig. 3 that the inclusion of the TKE equation in the set of model equations results in a much better agreement with observations over the entire range of surface Rossby numbers. This is especially true for logRo < 6.5, which is the range of Ro applicable to the tropics.

4. Height of maximum diffusivity

In problems of long-range transport of a pollutant, the choice of effective stack height is important. It would be interesting to calculate the height at which eddy diffusivity is maximum under neutral conditions, so that maximum dilution of a pollutant is achieved immediately on release.

From each set of model simulated velocity and diffusivity profiles, the height of maximum diffusivity ($h_{\max}$) and the corresponding (u_*/f) were obtained. Figure 4 shows a strikingly linear relationship between $h_{\max}$ and (u_*/f) viz.,

$$h_{\max} = 3.82 \times 10^{-2}(u_*/f) + 32.4$$

with a correlation coefficient of 0.99. Although such a relationship is implicit in Blackadar's (1962) work, no numerical relationship has so far been established. The use of this relationship and the one shown in Fig. 3 allow the height of maximum diffusivity corresponding to any given set of external parameters G, z_0 and f to be obtained and used in selecting stack heights for a given location. Here, $h_{\max}$ can be predicted with 99.9% confidence with a height range of $h_{\max} \pm 23$ m while, for 95% confidence, this range is ±12 m; $h_{\max}$ for $G = 8$ m s^{-1}, $z_0 = 1.0$ m and $f = 0.000071$ s^{-1} is 225 m.

5. Prediction of pollutant concentration patterns for different stack heights

In order to study how the concentration pattern changes within a selected domain, for different stack heights, under neutral stratification, the advection–diffusion equation has to be solved. Neglecting vertical advection and along-wind diffusion, the advection–dif-

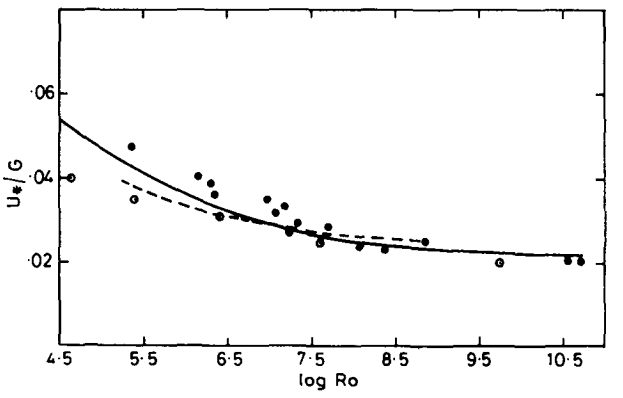

FIG. 3. Observed and predicted values of (u_*/G) as a function of log(Ro). Filled circles: results from experiments analysed by Csanady (1967). Solid line: present work. Dashed line: Estoque's (1974) model calculation. Open circles: calculated from Csanady's equation.

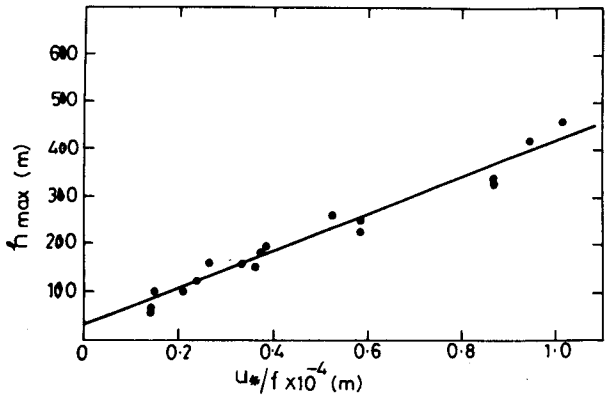

FIG. 4. Relation between (u_*/f) and h_{max}. Equation of the regression line is $h_{max} = 3.82 \times 10^{-2} (u_*/f) + 32.3$.

fusion equation (in the usual notation) can be written as

$$\frac{\partial c}{\partial t} + \frac{\partial}{\partial x}(cu) + \frac{\partial}{\partial y}(cv) = \frac{\partial}{\partial y}\left(K_y \frac{\partial c}{\partial y}\right) + \frac{\partial}{\partial z}\left(K_z \frac{\partial c}{\partial z}\right) + \frac{Q}{\Delta x \Delta y \Delta z}, \quad (6)$$

where Q is the source strength in $\mu g\ s^{-1}$ and c concentration in $\mu g\ m^{-3}$. In the first simulations, cross-wind diffusion was also neglected. In calculating concentration patterns it is assumed that at any instant the emission from the stack located at a fixed grid point is instantaneously diluted within the downwind parent grid. It is then dispersed to neighboring grids according to prevailing meteorological conditions.

With the velocity and diffusivity profiles obtained from the PBL model and specifying the source characteristics viz. source strength, source position and height, the set of equations are solved simultaneously using a Gaussian elimination method. The boundary conditions are (based on no inflow of flux from any of the boundaries)

$$u = 0, \quad v = 0, \quad K_z \frac{\partial c}{\partial z} = 0 \quad \text{at} \quad z = 0,$$

$$u = G, \quad v = 0, \quad K_z \frac{\partial c}{\partial z} = 0 \quad \text{at}$$

$$z = \delta \text{ (the PBL height).}$$

At the lateral boundaries,

$$\frac{\partial}{\partial x}(cu) = 0 \quad \text{at} \quad x = 0 \quad \text{and} \quad x = L,$$

$$\frac{\partial}{\partial y}(cv) = 0 \quad \text{at} \quad y = 0 \quad \text{and} \quad y = M.$$

Here L and M refer to the distances to the grid boundaries along the x and y directions respectively.

Initially a zero background concentration is assumed, and the model is integrated until a steady state solution is reached. A source strength of 750 g s^{-1} of SO_2 emission is used with a geostrophic wind velocity of 10 m s^{-1}. This source strength is typical of a power plant which is situated on the outskirts of Delhi. The model can output SO_2 concentrations in the x–z, x–y or y–z planes as desired.

In this study, the ground-level concentration (GLC) pattern is calculated for different surface roughness parameters and for different effective stack heights (H).

The following locations for the top of the stack were used in the simulation:

(i) the source is placed at the height h_{max} where K_{max} occurs ($H = h_{max}$);

(ii) the source is placed at one level above where K_{max} occurs ($H > h_{max}$); and

(iii) the source is placed at one level below the level where K_{max} occurs ($H < h_{max}$).

The maximum ground level concentration (GLC) and the distance at which it occurs are shown in Table 1 for different values of H and z_0. It is observed that as H increases by a factor of 2, the value of the maximum GLC decreases by a factor of 3. Over the whole range of roughness, it follows the relation

$$c_{max} \approx \frac{1}{H^{3/2}},$$

as shown in Fig. 5. It is observed from Table 1, that when the position of the stack is increased from a height which is one level below h_{max}, to the height of h_{max}, the value of maximum GLC reduces by a factor of approximately 2 and also the position of maximum GLC shifts to downwind distance by more than a factor

TABLE 1. Variation of GLC with surface roughness or different stack heights.

Surface roughness (z_0 (m))	Position of stack (m)	Max cu/Q ($m^{-2} \times 10^{-6}$) Without K_y	Max cu/Q ($m^{-2} \times 10^{-6}$) With K_y	Occurrence of max GLC (km) Without K_y	Occurrence of max GLC (km) With K_y
0.025	451.1	0.110	0.106	46.3	46.3
	289.9*	0.172	0.162	30.8	30.6
	171.2	0.338	0.330	10.5	10.5
0.1	387.4	0.141	0.132	45.7	45.7
	257.6*	0.217	0.207	20.8	20.8
	166.9	0.378	0.361	5.4	5.4
0.5	376.1	0.157	0.147	36.7	36.4
	253.4*	0.219	0.211	15.8	15.8
	253.8	0.389	0.381	5.4	5.4
1.0	314.0	0.225	0.217	21.2	21.2
	214.3*	0.275	0.270	10.8	10.8
	139.0	0.470	0.468	1.0	1.0

* Height at which K_{max} occurs, i.e., h_{max}.

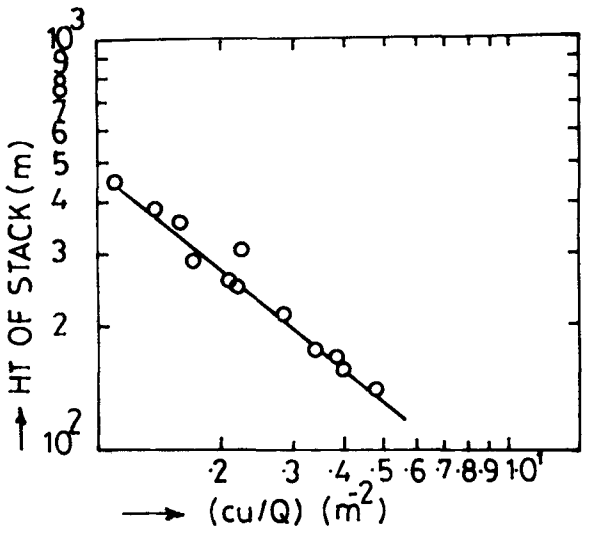

FIG. 5. Variation of concentration with height for different effective heights of stack and roughness lengths.

of 3 as shown in Fig. 6 where $c_{max} \propto H^4$. When the stack height is further increased from h_{max} to one level above it, maximum GLC reduces by a factor $\sim$ 1.6 while its location shifts downwind by a factor greater than 2. This shows that increasing the height of the stack up to a certain level (viz. height of K_{max}) decreases the GLC substantially while at the same time shifting the location of GLC further downwind. Increasing the stack height further (resulting in more expenditure) results in only a little more dilution and the position of maximum GLC occurs at a large distance from the source, making the pollutant part of a synoptic-scale system and increasing the danger of phenomena like acid rain. This result indicates without any ambiguity that the problem of airborn pollution cannot be solved by merely increasing the height of stacks. Increasing stack height not only increases initial costs, maintenance and design problems, but also makes pollution a regional if not a global menace. It is also observed that wherever the source is placed, with increasing roughness (or with increasing mechanical shear) the position of maximum GLC occurs nearer the stack. Also, the value of maximum GLC increases with increasing roughness as shown in Table 1. This was as expected. Fig. 6 shows the variation of position of maximum concentration for different effective heights of stack. It is observed that with increasing height of the stack there is a tendency of occurrence of maximum GLC further away, for all values of roughness.

The results obtained from the model were compared against the Gaussian model results (Wark and Warner, 1976). It is observed that under neutral stratification, for a selected effective height of stack, the value of maximum GLC is more by a factor of 3 in Gaussian models at the same downwind distance. This is as expected since it is well known that Gaussian models have a tendency to overpredict the ground-level concentrations. Thus, the usefulness of solving the full advection diffusion equation in impact assessment studies is highlighted.

Using the above formulation and solution, for any industrial plant, an appropriate height of the stack can be chosen for minimizing pollution. If an urban locality is present near the industrial complex, an optimal choice of height and location of the stack must be made, in addition to whatever other methods are used for minimizing the values of toxic material released.

6. Effect of lateral diffusivity (K_y)

For completeness, the effect of K_y on the GLC pattern is studied.

The numerical procedure outlined in the Appendix is followed by setting $K_y = 2K_z$ (Yu, 1977).

It is observed that there is practically no differences in the GLC pattern after inclusion of K_y. The computer time required for convergence to set in is about 6.3 min in ICL 2960 system. Although, there is a marginal difference in the maximum GLC value, there is no difference in the position of maximum GLC. After increasing the value of K_y arbitrarily to $K_y = 20K_z$, there is no major change in the values as listed in Table 1 and Table 2.

The effects of K_y and K_z are studied separately. It is observed that when there is no vertical dispersion, there is no concentration at the ground level with pollutants dispersing only in the x–y plane, as intended. Moreover, it is observed that the vertical dispersion process is a faster process compared to the lateral dispersion process.

From the two contour plots of ground level concentration, viz., with and without inclusion of K_y (Figs. 7a and b) the following conclusions could be drawn:

(i) An overall dilution of concentration occurs throughout the domain of interest when K_y is intro-

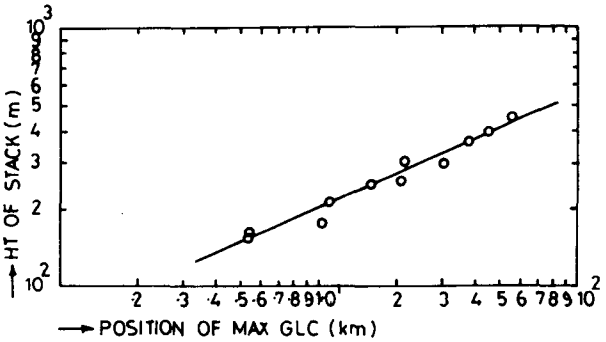

FIG. 6. Variation of position of maximum concentration for different effective heights of stack.

TABLE 2.

Surface roughness (z_0 (m))	Height of stack (m)	Max GLC ($\mu g/m^3$)				Occurrence of max GLC (km)			
		With K_z only	$K_y = 5K_z$	$K_y = 10K_z$	$K_y = 20K_z$	With K_z only	$K_y = 5K_z$	$K_y = 10K_z$	$K_y = 20K_z$
1.0	214.3	26.5	24.5	22.8	20.0	10.8	10.5	10.3	9.4

duced. However, this dilution is marginal, the maximum dilution being a factor of 1.08. This occurs at a distance of 18–29 km from the source.

(ii) The contour plot of concentrations obtained with the inclusion of K_y also shows clearly the spread of the plume in the lateral direction.

To summarize, the velocity and diffusivity profiles from the neutral PBL model are used in studying the dispersion of pollutants, by solving a three-dimensional advection diffusion equation. The study shows that

1) The maximum ground level concentration decreases as $H^{-3/2}$ where H is the effective stack height.

2) The location, of maximum ground level concentration from the stack increases as H^4.

3) Increases in roughness both increases the GLC and decreases the distance of its location from the stack.

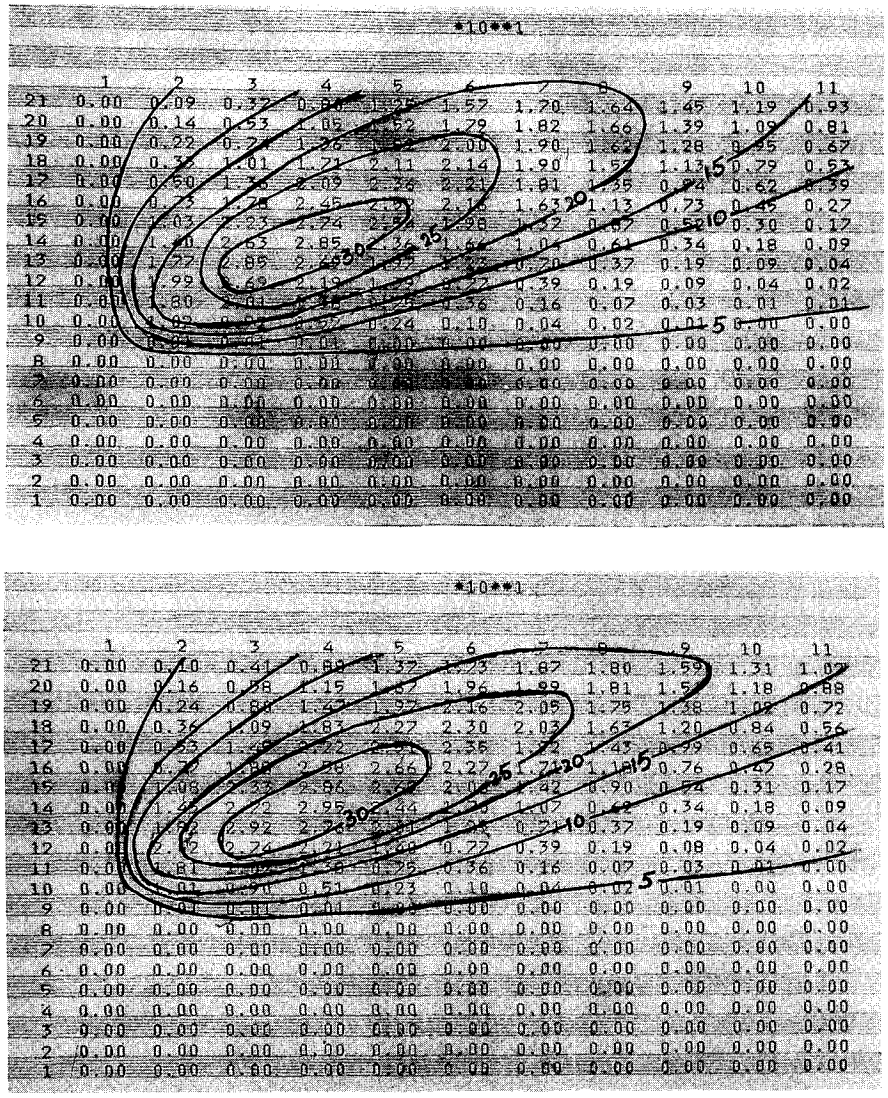

FIG. 7. (a) Computer contour plot of the GLC pattern when K_y is introduced.
(b) Computer contour plot of the GLC pattern with K_z only.

4) The inclusion of crosswind diffusion has only a negligible effect on ground-level concentration due to a polluting source located high above the ground.

5) The advection diffusion model predicts ground-level concentration one-third that predicted by a Gaussian model emphasizing the need to solve the three-dimensional advection diffusion equation for realistic results.

7. Conclusions

The present study uses the turbulent kinetic energy equation along with the momentum equations to obtain the wind and diffusivity profiles in the neutral planetary boundary layer. Model predictions of wind speed and direction compare favorably with routine radiosonde observations at 10- and 500-m heights. The model is also able to predict very satisfactorily the observed relationship between geostrophic drag coefficient and surface Rossby number. A well-defined correlation between the height of maximum diffusivity and the length scale (u_*/f) of the planetary boundary layer is established. This relationship could be valuable in choosing stack heights to minimize long-range transport of pollutants. These conclusions should greatly assist in the siting of new industrial complexes and in other aspects of town planning.

Acknowledgments. It is our pleasant duty to thank professor M. P. Singh for his constant support. Thanks are due to Dr. B. Johns for his clarifications regarding the numerical scheme for the transport of pollutants. We are grateful to Professor K. S. Rao for his critical review of the work. Thanks are also due to Dr. L. Gutman for his meticulous review of the manuscript and valuable suggestions, which have improved the quality of this work to a very great extent.

APPENDIX

Numerical Schemes for the Differential Equations

The set of equations in the PBL are solved in a transformed coordinate system along the vertical. A log-linear transformation was found to be most appropriate, which is given by

$$\zeta = \ln\left(\frac{z + z_0}{z_0}\right) + \frac{z}{z_1}, \tag{A1}$$

where

z_0 roughness length; $z_1 = 500$ m
ζ is the transformed coordinate

The set of momentum equations and the turbulent kinetic energy equation is solved after writing the equation in the centered difference form in space and implicit form in time, e.g., the first momentum equation is written as

$$\frac{\partial u}{\partial t} = f(v - v_g) + \frac{\partial}{\partial z}\left(K_m \frac{\partial u}{\partial z}\right)$$

$$\frac{u_j^{n+1} - u_j^n}{\Delta t} = f(v_j^{n+1} - v_g) + \left[\left(K\frac{\partial u}{\partial z}\right)_{j+1/2}^{n+1} - \left(K\frac{\partial u}{\partial z}\right)_{j-1/2}^{n+1}\right]$$

$$= f(v_j^{n+1} - v_g) + \left[\left(\frac{K_j^{n+1} + K_{j+1}{}^{n+1}}{2}\right) \times \frac{u_{j+1}{}^{n+1} - u_j^{n+1}}{(\Delta z)^2} - \left(\frac{K_j^{n+1} + K_{j-1}{}^{n+1}}{2}\right)\frac{u_j^{n+1} - u_{j-1}{}^{n+1}}{(\Delta z)^2}\right]. \tag{A2}$$

Regarding the discretization of the diffusion term, the first difference of the variables is obtained at the half levels as shown so that the second difference is automatically obtained at the levels where the values of the rest of the variables are known.

The equation for the advection and diffusion of pollutant concentration is solved numerically using a finite difference scheme. The equation is given by

$$\frac{\partial c}{\partial t} + u\frac{\partial c}{\partial x} + v\frac{\partial c}{\partial y} = \frac{\partial}{\partial z}\left(K_z\frac{\partial c}{\partial z}\right)^2 + \frac{Q}{\Delta x \Delta y \Delta z}. \tag{A3}$$

The advection term is written in the flux form entirely and an upwind difference scheme is utilized. The product cu (flux) is differentiated so that the matter generally is conserved. Thus, the advection term is written as

$$\left[\frac{\partial}{\partial x}(cu)\right]_{ijk}^n = \frac{1}{2\Delta x}[f_{ijk} - |f_{ijk}|]c_{(i+1)jk}{}^n + [f_{ijk} + |f_{ijk}| - g_{ijk} + |g_{ijk}|]c_{ijk}{}^n + [-g_{ijk} + |g_{ijk}|]c_{(i-1)jk}{}^n. \tag{A4}$$

The superscripts refer to the time level and the subscripts refer to the space level. Hence,

$$\left.\begin{aligned} f_{ijk} &= \frac{u_{ijk}{}^n + u_{(i+1)jk}{}^n}{2}, \\ g_{ijk} &= \frac{u_{ijk}{}^n + u_{(i-1)jk}{}^n}{2} \end{aligned}\right\}.$$

As is evident from (A4) the concentrations in the grids are weighted appropriately so that the pollutants are never advected in the upwind direction. The scheme is also very useful since it is capable of handling the reversal in the wind direction (Johns, private communication, 1981) properly.

The log-linear coordinate transformation is applied along the vertical in the advection difference equation so that the concentrations are calculated at the same grid points as those at which the flow parameters are computed. The numerical grid consists of 11×21 grid

points in the horizontal covering a domain of 50 km $\times$ 20 km such that Δx = 5 km and Δy = 1 km; 21 levels are used in the vertical extending to a height of 2 km. It takes about 4.8 min for convergence to occur in the ICL 2960 system.

REFERENCES

Blackadar, A. K., 1962: The vertical distribution of wind and turbulent exchange in neutral atmosphere. *J. Geophys. Res.*, **67,** 3095–3102.

Csanady, G. T., 1967: On the resistance law of a turbulent Ekman layer. *J. Atmos. Sci.*, **24,** 467–470.

Delage, Y., 1974: A numerical study of the nocturnal atmospheric boundary layer. *Quart. J. Roy. Meteor. Soc.*, **100,** 351–364.

Draxler, R. R., 1979: An improved gaussian model for long term average air concentration estimates. *Atmospheric Environment,* **14,** 597–601.

Estoque, M. A., 1974: Numerical modelling of planetary boundary layer. Am. Met. Soc. Workshop on Micrometeorology, pp. 217–270.

Nieuwstadt, F. T. M., and A. G. M. Driedonks, 1979: The nocturnal boundary layer: A case study compared with model calculations. *J. Appl. Meteor.*, **18,** 1397–1405.

Padmanabhamurty, B., and R. N. Gupta, 1978: Changes in turbulent diffusion and mixing depth in rural and urban Delhi. Proceedings of the International Symposium on Environmental Agents and their Biological Effects. Bangalore, India pp. 83–86.

Rao, K. S., and H. F. Snodgrass, 1981: A nonstationary nocturnal drainage flow model. *Bound. Layer Met.*, **20,** 309–320.

Wark, K., and C. F. Warner, 1976: Air pollution its origin and control. Harper and Row.

Yu, T., 1977: A comparative study on parameterization of vertical turbulent exchange processes. *Mon. Wea. Rev.*, **105,** 57–66.